Optical test bench experiments for 1-Tb/s satellite feeder uplinks

Karim Elayoubi, Angélique Rissons, Aniceto Belmonte

Optical test bench experiments for 1-Tb/s satellite feeder uplinks

K. Elayoubi [a b], A. Rissons [b], A. Belmonte [c]
[a] Institut of Technology Antoine de Saint Exupéry, CS 34436, 3 Rue Tarfaya, 31400 Toulouse
[b] Dept. of Electrical, Optronics and Signal, Institut Supérieur de l'Aéronautique et de l'Espace, 10 Avenue Edward Belin, 31400 Toulouse
[c] Univ.Politècnica de Catalunya, Barcelona, Spain

ABSTRACT

Due to expected capacity bottlenecks of exploited microwave technologies, feeder links for data relay or broadband access systems will require the implementation of high capacity optical communication links between space and ground. In this context, it is necessary a detailed investigation of the optical technologies and techniques that could enable the transmission of high data rates at optical frequencies through the Earth's atmosphere, with regard to all kinds of atmospheric phenomena. In particular, the adverse effects of atmospheric turbulence fading are of special relevance to optical communication systems for ground-to-space uplink applications. Although previous studies and experiments have demonstrated the feasibility of such optical links at low data rate, research is still needed to identify technical solutions and strategies adapted to the specific constraints imposed to these high-speed links in order to ensure the required level of performance. Against this background, various test benches have been developed in order to characterize different modulation and detection techniques for optical communication systems prior to be incorporated in the conceptual design of future 1-Tb/s ground-space optical links. The expected performances of such an experimental demonstration are derived based on simulation models taking into account atmospheric turbulence effects, in order to prove the feasibility of reliable ground-space high date rate optical communication links. Our first simulation studies, considering On-Off Keying (OOK) and Differential Phase Shift Keying (DPSK) modulations, have allowed us to understand the complexity of the link and to optimize both the transmitter and the receiver to achieve acceptable performance levels.

Keywords: Optical modulation, Feeder uplinks, Atmospheric propagation, Free space optical communication, Time series

1. INTRODUCTION

Satellites telecommunications must follow the advances of terrestrial network capacities and increase data rate and performances to remain competitive. In comparison with radio communication systems, space optical communication have advantages such as a large bandwidth available, power efficient, lower size and weight of terminals, no interference with other waves and no frequency regulation. Despite these advantages, space optical communications suffer from a stronger atmospheric perturbation (turbulence and cloud), eye safety issues (due to the highest power needed to establish the communication) and the requirement of accurate pointing system. To solve saturation radiofrequency bandwidth, study proved the feasibility of this kind of communication [1][2]–[6] and now the challenge is to improve the quality, data rate and performances to achieve 1Tbit/s data rate. According to optical communication standard, several working area are possible to reach goals such as modulation formats and coding, signal noises, spatial acquisition procedure and optical tracking.

During the atmospheric propagation (uplinks or downlinks), the optical beam is deflected (beam wandering), and possibly distorted (beam spreading), by atmospheric turbulence. Consequently, the detected signal presents a strong fluctuation and can induce pointing errors that increase the bit error rate (BER). One of the candidate solutions to correct these effects is the adaptive optics (AO) that is a mature technology used on astronomy and biomedical application. Considering the uplink, it consists consist on modifying the beam characteristics at the emission to pre-compensate the beam deformations.

This paper goes through various details of an end-to-end free space optical (FSO) communication emulator that we developed to emulate a ground-to-LEO satellite scenario in different turbulence cases. Section 2 present the design of

Laser Communication and Propagation through the Atmosphere and Oceans VII, edited by Jeremy P. Bos, Alexander M. J. van Eijk, Stephen Hammel, Proc. of SPIE Vol. 10770, 1077006
 · doi: 10.1117/12.2317728

communication link and theirs performances using an OOK modulation at 10 Gbps. Section 3 discuss the propagation channel condition and the theoretical part used to generate time series of realistic atmosphere propagation (high turbulences and low turbulences). The end-to-end optical links assessment and theirs communications quality are considered in Section 4. Then we conclude with Section 5.

2. ATMOSPHERIC PROPAGATION CHANNEL

2.1 Description of the atmospheric turbulence

The air temperature fluctuations cause local refractive index variations which are neither constant nor homogeneous along the propagation line of sight. In addition, these refractive index fluctuations are characterized with their power spectral density. The variability of the refractive index is estimated by the refractive index structure parameters C_n^2 which corresponds to the variance of the refractive index between two points separated by one meter and can also characterize the turbulence strength. When the vertical path is considered, as in a feeder link scenario, the C_n^2 parameter is mainly affected by temperature changes along the different layers within the Earth's atmosphere. Consequently, it becomes a function of the height h above the ground level and the widespread C_n^2 profile model is the Hufnagel-Valley profile [7] defined by :

$$C_n^2(h) = 0.00594 \times (\frac{v}{27})^2 (10^{-5}h)^{10} e^{-\frac{h}{1000}} + 2.7 \times 10^{-16} e^{-\frac{h}{1500}} + C_g e^{-\frac{h}{100}} [m^{-2/3}]$$

Where $C_g = 5.4 \times 10^{-14} m^{-2/3}$ is the refractive index structure parameter at ground level, h is the altitude and $v = 21$ m/s is the root-mean-squared wind speed. These values correspond to a strong turbulence case for 1550 nm wavelength [7] [8].

2.2 Description of the wind profile

The wind profile that will be used in this propagation model is the classical Bufton profile [7] in which the atmospheric layers move with 5 m/s speed at ground level (S_G) and with 25 m/s speed at an altitude of 10 km (H_p). The wind speed $V(h)$ is given as an expression of S_G , H_p and W_P = 4800 m :

$$V(h) = V_G + V_P e^{-(\frac{h-H_P}{W_P})^2}$$

2.3 Optical ground station

We will admit in this paper that the optical beam generated at the optical ground station (OGS) is a Gaussian laser beam of waist size of ω_0 and the total diameter of the beam is two time this waist size ($D_{Beam} = 2\ \omega_0$). We also admit that the emitted Gaussian beam is considered collimated until the exit of the emitter pupil. Figure 1 describes these parameters:

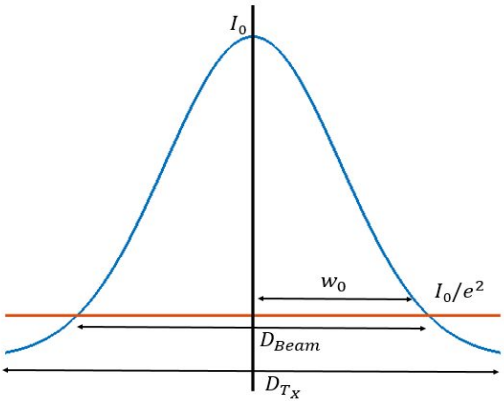

Figure 1 : Gaussian beam parameters

2.4 Waist effect

According to the Freid parameter, r_0 [9], if the waist is smaller than r_0 ($\omega_0 << r_0$), the waist become less sensitive to the atmospheric turbulence effects. However, the lower waist is, the higher the divergence is. As a conclusion, a trade-off will have to be found to achieve the targeted power detected by the satellite.

2.5 Statistical model for irradiance fluctuation and its validity domain

The fluctuation model we use is from Baker's model [10] that used the low-order turbulence (LOT) phase fluctuations developed for Gaussian beams in the weak scintillation regime. In fact, the LOT solution take into account the irradiance statistics to describe the movement of the Gaussian beam in front of the satellite detecting pupil. In other words, Baker proposes to describe the irradiance fluctuations of the beam propagation only using the first and second Zernike polynomials: Tip/tilt, defocus and astigmatism [11]. Some modifications and improvements are added to Baker's model to take into account the effects of the outer scale and the beam diffraction due to the size of emitting telescope compared to the infinite Gaussian beam. For the validity of our model, if we tolerate that the residual mean square phase error between our model and TURANDO model [12] to be less than 10%, this gives the validity regime of the model of $\omega_0 < 1.5r_0$. More detail about this uplink model can be found in [13].

2.6 Adaptive optics compensation

The adaptive optics (AO) system is a servo system which modifies in real time the emitted wave front in order to pre-compensate the wave front deformation due to atmospheric turbulence. This technique allows us to have an unperturbed waveform when reaching the satellite. In addition, due to the Earth's rotation during the beam's propagation, the point-ahead angle (PAA) between the downlink and the uplink is considered and make the turbulences effects slightly different. As a result, these effects have to be taken into account for the AO system to insure the right pre-compensation for each case (uplink or downlink). In our simulation, we will take a PPA value of 18.5 µrad, usually considered for European latitudes. Figure 2 shows the simplified principle of adaptive optics in case of plane waves.

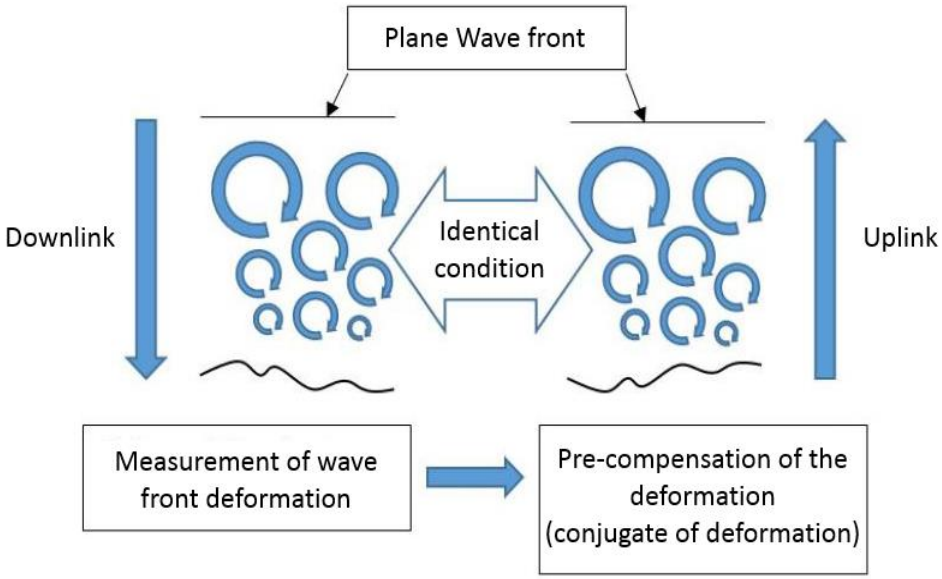

Figure 2 : Adaptive optics correction in case of plane waves

Figure 3 shows the received optical beam in both conditions, adaptive optics correction and no-correction.

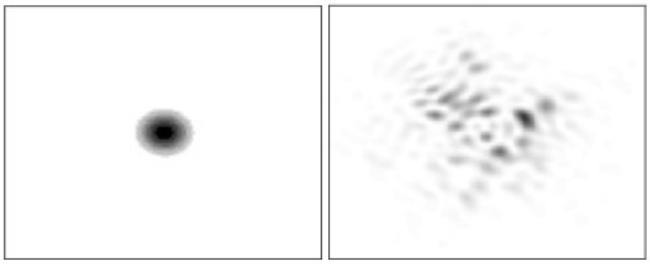

Figure 3 : Advantages of adaptive optics correction. Left: with correction. Right: without correction [14].

After introduction the phase screen deformation to the Gaussian beam, we implement an adaptive optics system to correct these deformations by pre-compensating it. We will show here after the adaptive optics effect on the received power and on the system capacity.

2.7 Time series

We are now able to generate very long sequences of random irradiances and able to predict the irradiance fluctuations detected by the satellite. For next parts, we will focus on the average power received at the satellite with our model. Two uplink scenarios will be considered: mitigation with tip/tilt compensation and mitigation with no correction. Figure 4 shows both of correction and non-correction cases.

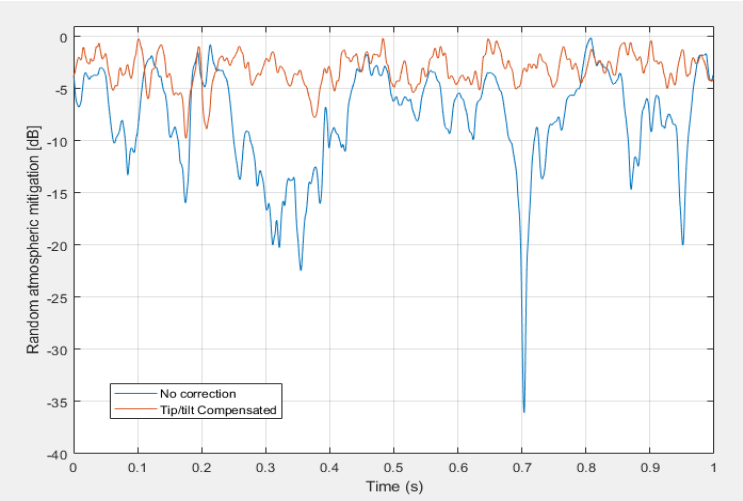

Figure 4 : Example of time series of random atmospheric mitigation with 2000 Hz sampling (ω_0=8cm & PPA = 18 µrad)

For the next parts, we will consider both of these times series to drive the propagation channel part and compare simulation and experiment performances. We will now define the communication link used to validate an end-to-end FSO scenario that we developed for this application.

3. OPTICAL COMMUNICATION MODELING

3.1 Optical link simulation

The optical communication link is divided in three parts: the transmitter, the propagation channel emulator and the receiver. The transmitter is designed to generate an On Off Keying (OOK) modulation with 10 Gbps data rate. The data used is a pseudo random binary sequence (PRBS) with 2^{31}-1 length. In addition, two different duty cycles can be considered for this transmitter: Non-Return-to-Zero (NRZ) and 50% RZ OOK thanks to two Mach Zehnder Modulator (MZM). More information about this communication transmitter can be found in [15].
The propagation emulator channel is modeled by two different variable optical attenuators (VOA): the first is used to introduce the atmospheric attenuation and all static mitigation, the second one is to emulate the random mitigation due to phase screen deformation (Tip/Tilt) and its correction with adaptive optics system.

The receiver is composed of an optically pre-amplification part and detection part. After receiving the optical power, it goes through an Erbium Doped Fiber Amplifier with low noise factor (LNOA) before using a passband optical filter to suppress to the accumulation of the background noise and the Amplified Spontaneous Emission (ASE) noise generated by the amplifier. Then, the signal is sent to PIN photo-detection and a low pass filter in order to cut high frequencies and limit the electrical noise. Figure 5 shows these components. All filtering effects are optimized with signal processing technics and adapted filtering in order to improve the bit error rate (BER).

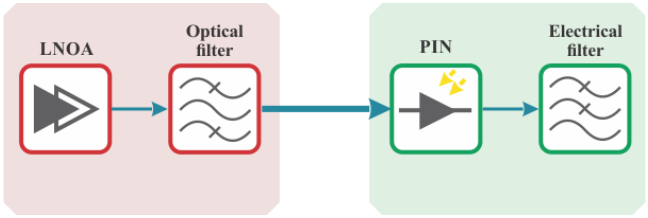

Figure 5 : Pre-amplified optical receiver

Table 1 summarize the main transmitter and receiver parameters.

Transmitter		Receiver	
Wavelength communication	1550 nm	EDFA Preamplifier	
CW Laser		Gain	20 dB
Linewidth	10 MHz	Noise figure	5 dB
RIN	-150 dB/Hz	Optical filter	
NRZ coder		Type	Gaussian
Rise/fall time type	Raised-cosine	Filer order	1
Rise/fall time duration	22 ps	Bandwidth	Optimized
Jitter duration	1.1 ps	Photodiode	
MZM		Responsivity	0.9 A/W
Extinction ration	25 dB	Dark current	0 nA
Insertion loss	4 dB	Thermal noise	10 pA/(Hz)$^{0.5}$
Bias transmission	50%	Electrical filter	
Booster amplifier		Type	Low-pass Bessel 5th order
Gain	20 dB	Bandwidth	Optimized
Noise figure	6 dB		

Table 1 : Transmitter and receiver parameters used for the optical link

After describing the communication link and the main components parameters, we will verify in the next part their performances.

3.2 Link performances

To assess our communication link, three parameters will be considered: Average input power at the receiver, fading time introducing by the atmospheric propagation and the BER.
First, we start to assess the receiver by measuring BER of received data for a linear attenuation. In fact, to estimate the BER, we used the Gaussian statistical model assuming that the statistics of the received optical signal are Gaussian and the decision threshold is continuously optimized to have the best BER value. We consider both of NRZ and RZ optical modulation with three different duty cycles (33%, 50% and 67%). An analysis done by Winzer and Klamar [16] prove that the maximum of sensitivity improvement can be obtained for low duty cycles in an optically preamplified receiver and the filtering step has an important role to achieve this improvement. They also conclude that choosing the optical filter bandwidth much larger that both the electrical bandwidth and signal bandwidth lead to get the best sensitivity of such receivers for noise optimization reasons. In fact, it is due to the amplified spontaneous emission (ASE) filtering that takes place before the square law detector which reduces the level of ASE-ASE beat noise. Thereby our simulation study was focused especially in these link parameters. Figure 6 illustrate BER curves as a function of average input power for NRZ and RZ with different duty cycles.

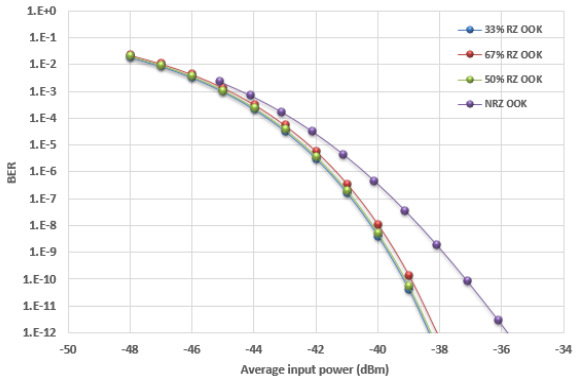

Figure 6: BER curves vs. average input power for NRZ and RZ with different duty cycles

For 10 Gbps transmissions, optically pre-amplified, single mode receiver architectures are the most practical as the components are widely available and near quantum limited sensitivities have been achieved [17]. The ideal average power for an ideal preamplifier receiver at 10 Gbps is around 38 photons per bit (ppb) for 10^{-9} of BER, which corresponds to -43 dBm. Several experiments were done to evaluate the receiver sensitivity and most of them give values between -40 dBm and -37 dBm at 10 Gbps for a BER of 10^{-9} in [17],[18], [19] and [20]. We achieved with our communication link a receiver sensitivity of – 38 dBm for NRZ. This value changes highly (± 2 dBm) by modifying any optical link parameter such optical bandwidth, electrical bandwidth, thermal noise, etc. In addition, Figure 5 shows that reducing the duty cycle permit to increase the sensitivity the receiver due its low intersymbol interferences (ISI) between adjacent bits. Furthermore, we note that for the RZ modulation, the sensitivity gain obtained by reducing the duty cycle is very low because of the value of the rise/fall times and jitter used for simulation links. Hence, the decision time for short duty cycles seems to be more difficult compared to NRZ OOK modulation which can explain the low difference between 33%, 50% and 67% RZ OOK BER curves. To make the comparison between simulation and experiments values, we need to be on the same conditions for both. All simulation parameters are chosen to match with components that we use on the optical bench.

3.3 Optical test bench

The optical test bench that we developed in the farme of IRT-ALBS project is designed to work with both of OOK and DPSK modulations but the DPSK modulation is not considered hereafter. The figure 7 show a global view of the optical bench.

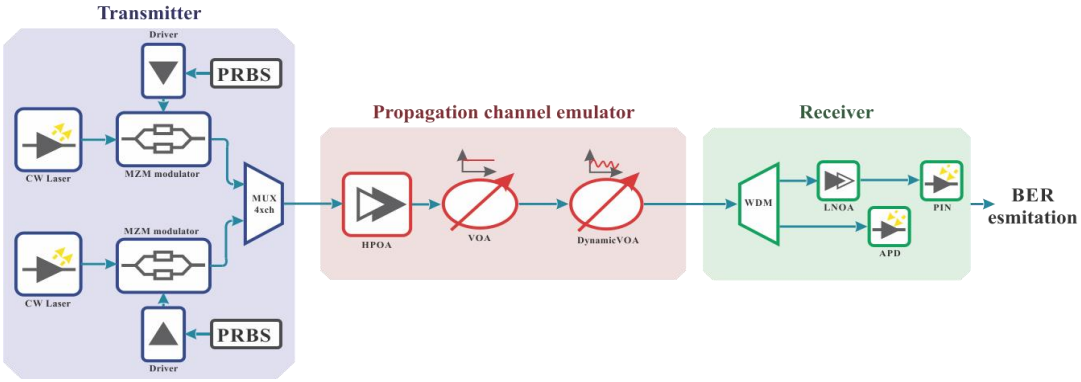

Figure 7 : Optical test bench scheme and its components used for OOK modulation

The transmitter side contains two continuous wave lasers that feed two electro-optical modulators: the first one used to transfer data onto the optical carrier while the second one is used to generate the optical pulses. Two modulator drivers are used to in order to drive the modulator with the relevant signal features. The next component is the booster amplifier which raises the power of the signal before emission to a level compatible with the receiver sensitivity after losses associated to the propagation channel. This configuration can be used to generate the RZ modulation by cascading both of MZM modulators. In this case, the second modulator is known as the pulse carver and it is driven by periodically electrical signal. The phase shift between data signal and the pulse carver signal has to be managed and reduced to insure the desirable duty cycle.

The propagation channel is implemented using fiber optic components in the first version of the bench. This part is achieved by cascading two variable optical attenuators. The first one is used to represent average propagation losses variation during FSO communication. Its attenuation's value is fixed or slowly varying to represent these losses. The second one whose attenuation is driven by an electrical signal provided from time series detailed in section 2.7.

The receiver sub-system includes a low noise optical amplifier (LNOA), a WDM demultiplexer that we use as Gaussian optical filter and PIN photo-receiver detector. It also contains an Avalanche photo-receiver (APD) that we use to compare its sensitivity with preamplifier PIN.

The BER is estimated using the Gaussian method that consist on calculating the average levels and variance of 'one' and 'zero' bits. The decision threshold is calculated relative to the signal levels which defined as a fraction value between

received ‘one’ and ‘zero’ bits. Our objective of BER value is 10^{-9} that we consider as an error free communication. In addition, we can consider BER values between 10^{-9} and 10^{-3} that could be recovered using interleaving and error code correcting techniques [21], [22]. The BER experimental values are shown in figure 8.

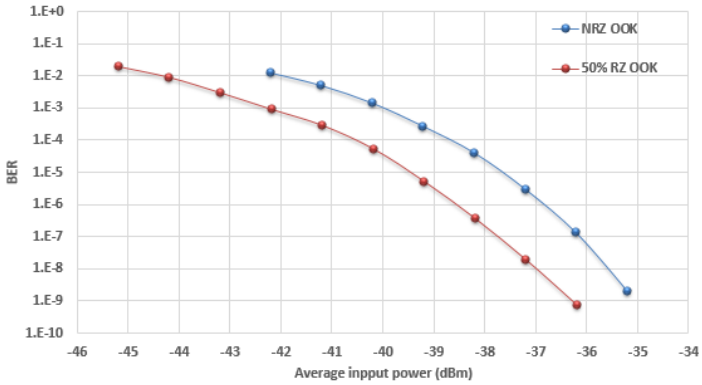

Figure 8 : Transmitter and receiver design used for the optical bench

Before describing these curves, we have to take into account experimental conditions and the deviation of some components which promote to increase the BER. An estimation of ±1dB around experimental values has to be considered due to environmental conditions effects. In addition, the use of the electrical filter in post detection on the simulation model permits to limit the cumulated noise in the whole optical link before the making the decision. Hence, we can show a difference value up to 2.5 dB. Table 2 shows the sensitivity comparison between model and experiments:

Modulation	RZ-33%	50%	67%	NRZ
Simulation model	-39.7 dBm	-39.6 dBm	-39.3 dBm	-38 dBm
Experiments	NA	-36.4 dBm	NA	-35.5 dBm

Table 2 : Sensitivity comparison between experiment and simulation model at 10^{-9} BER.

Then, we have driven the second optical attenuator of the propagation channel part with times series in both cases (simulation and experiment) to emulate free space optical mitigation. 33% and 67% duty cycles experiments results will be presented in a future paper.

3.4 End-to-end free optical link model.

After generating the times series and having the optical link optimized, we driven the dynamic VOA with times series values. We consider here that all static mitigations were taken into account on by the first VOA the optical propagation channel. In this study we will only focus on fading time induced by times series on the receiver and the BER is estimated for each sample over a duration of 500 µs, assuming that the irradiance is constant over this time period. Two threshold levels are chosen (power sensitivity for BER equals to 10^{-3} and for BER equals to 10^{-9}) and we consider that the communication is near the error free for 10^{-9} BER value and below. For average power between these levels, the data can be recovered by using forward-error correcting code (FEC) such as Low-Density Parity-Check (LDPC) code designed by the NASA and which is a part of the CCSDS recommendations for deep-space telemetry application [23]. The worst case is when the average power is above 10^{-3} BER level where we can not recover any data.

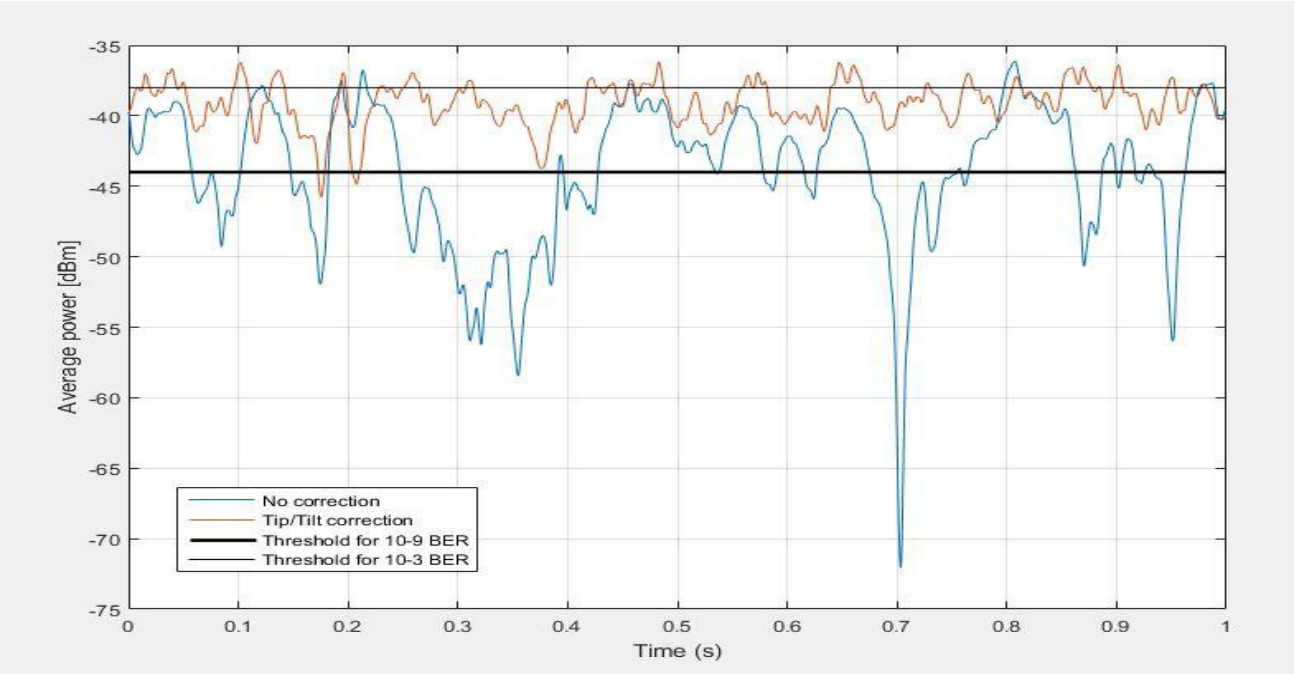

Figure 9: Time fading estimation for both of Tip-Tilt correction and no-correction with NRZ thresholds.

On the case of non-correction, we remark that atmospheric turbulences have a strong effect on the optical beam during the propagation illustrated with high optical mitigation. In addition, the received signal spends the big part of 1s under the acceptable threshold for the no-correction case. Table 3 summarizes the estimations of fading time over 1s time series in both cases and for two duty cycles:

	No-Tip/Tilt correction			**Tip/Tilt correction**		
	Average power (dBm)	**Fading time (%)**		**Average power (dBm)**	**Fading time (%)**	
Duty cycle (%)		**NRZ**	**50% RZ**		**NRZ**	**50% RZ**
Power threshold @ BER = 10^{-3}	-39.1	44.15%	35.30%	-30.3	1.3%	0.4%
Power threshold @ BER = 10^{-9}		95.85%	80.85%		78.30	37.20%

Figure 9 show the importance to use the Tip/Tilt correction to improve the atmospheric attenuation effects. According to these results, the correction present the smallest fading time that achieves 1.3% of total time propagation for NRZ link and 0.4 % for RZ link with 10^{-3} threshold. In addition, we remark that reducing the duty cycle leads to improve the time which corresponds to theoretical improvement offered by RZ pulses. One of the worst cases is the NRZ with 10^{-9} threshold because it has the poorest sensitivity compared to the pointing error effects and tracking error during the communication link between the OGS and satellite induced by the atmosphere layers.

3.5 Perspectives

To complete our experimental model, we plan to switch to a free space optical part that includes the wave front deformation, optical beam collimation, adaptive optics loop and single mode fiber injection. All system and results from this part will be presented in a next paper. Once this step is done, a WDM system will be implemented to multiplex up to 4 carriers around 1550 nm on the aim to achieve high data rate.

4. CONCLUSION

Our first simulation studies, considering On-Off Keying (OOK) and Differential Phase Shift Keying (DPSK) modulations, have allowed us to understand the complexity of the link and to optimize both the transmitter and the receiver to achieve acceptable performance levels. Optical feeder links is essential to increase data throughput in telecommunication satellites to achieve 1 Tb/s. This work demonstrated the importance of satellite tracking by correcting Tip/Tilt effect using pre-compensation which can change seriously performances of transmission. In addition, the optical link specifications are very important to be optimized on the aim to reduce time fading. We achieved 0.4% of fading time rate for 1s atmospheric propagation using the 50% RZ modulation and pre-compensating the Tip/Tilt effects. Otherwise, the total fading time rate is equal to 35.30% when the pre-compensation is not considered. The lost data on the communication is depending directly on this fading time and we can recover a part of them by using error correcting code. This simulation study, considering On-Off Keying (OOK) modulations, allowed us to understand the complexity of the link and to optimize both the transmitter and the receiver to achieve acceptable performance levels.

REFERENCES

[1] Z. Sodnik, B. Furch, and H. Lutz, "Free-Space Laser Communication Activities in Europe: SILEX and beyond," in *2006 IEEE LEOS Annual Meeting Conference Proceedings*, 2006, vol. 1, no. March 2003, pp. 78–79.

[2] T. Tolker-Nielsen and J.-C. Guillen, "SILEX : The First European Optical Communication Terminal in Orbit," *ESA Bull.*, vol. 96, no. november, 1998.

[3] V. Cazaubiel, G. Planche, V. Chorvalli, L. Le Hors, B. Roy, E. Giraud, L. Vaillon, F. Carré, and E. Decourbey, "Lola : a 40 . 000 Km Optical Link Between an Aircraft and a Geostationary Satellite," vol. 2006, no. June, pp. 27–30, 2006.

[4] Y. Koyama, M. Toyoshima, Y. Takayama, H. Takenaka, K. Shiratama, I. Mase, and O. Kawamoto, "SOTA: Small Optical Transponder for micro-satellite," *2011 Int. Conf. Sp. Opt. Syst. Appl. ICSOS'11*, pp. 97–101, 2011.

[5] C. Petit, V. Nicolas, C. Petit, and V. Nicolas, "Investigation of adaptive optics performance through propagation channel characterization with the Small Optical TrAnsponder SOTA eraldine Artaud , Etienne Samain , Morio Toyoshima To cite this version :," 2016.

[6] H. Kaushal and G. Kaddoum, "Optical Communication in Space: Challenges and Mitigation Techniques," *IEEE Commun. Surv. Tutorials*, vol. 19, no. 1, pp. 57–96, Jan. 2015.

[7] J. W. Hardy, *Adaptive Optics for Astronomical Telescopes*. Oxford University Press, 1998.

[8] S. Dimitrov, B. Matuz, G. Liva, R. Barrios, R. Mata-Calvo, and D. Giggenbach, "Digital modulation and coding for satellite optical feeder links," *2014 7th Adv. Satell. Multimed. Syst. Conf. 13th Signal Process. Sp. Commun. Work. ASMS/SPSC 2014*, vol. 2014-Janua, pp. 150–157, 2014.

[9] D. L. Fried, "Optical Resolution Through a Randomly Inhomogeneous Medium for Very Long and Very Short Exposures," *J. Opt. Soc. Am.*, vol. 56, no. 10, p. 1372, 1966.

[10] G. J. Baker, "Gaussian beam weak scintillation: low-order turbulence effects and applicability of the Rytov method.," *J. Opt. Soc. Am. A. Opt. Image Sci. Vis.*, vol. 23, no. 2, pp. 395–417, 2006.

[11] R. J. Noll, "Zernike polynomials and atmospheric turbulence*," *J. Opt. Soc. Am.*, vol. 66, no. 3, p. 207, 1976.

[12] N. Védrenne, J. M. Conan, M. T. Velluet, M. Sechaud, M. Toyoshima, H. Takenaka, A. Guérin, and F. Lacoste, "Turbulence effects on bi-directional ground-to-satellite laser communication systems," *Proc. Int. Conf. Sp. Opt. Syst. Appl.*, vol. 12, 2012.

[13] A.-R. Camboulives, M.-T. Velluet, S. Poulenard, L. Saint-Antonin, and V. Michau, "Optical ground station optimization for future optical geostationary satellite feeder uplinks," in *SPIE LASE*, 2017, vol. 1009608, no. February, p. 1009608.

[14] N. Perlot, T. Dreischer, C. M. Weinert, and J. Perdigues, "Optical GEO feeder link design," *2012 21st Futur. Netw. Mob. Summit, Futur. 2012*, pp. 1–8, 2012.

[15] K. Elayoubi, A. Rissons, J. Lacan, L. Saint Antonin, M. Sotom, and A. Le Kernec, "RZ-DPSK optical modulation for free space optical communication by satellites," in *IEEE 2017 Opto-Electronics and Communications Conference (OECC) and Photonics Global Conference (PGC)*, 2017, no. 1, pp. 1–2.

[16] P. J. Winzer and A. Kalmár, "Sensitivity Enhancement of Optical Receivers by Impulsive Coding," *J. Light. Technol.*, vol. 17, no. 2, pp. 171–177, 1999.

[17] D. O. Caplan and W. A. Atia, "A quantum-limited optically-matched communication link," *Ofc*, vol. 1, p. MM2, 2001.

[18] W. a. Atia and R. S. Bondurant, "Demonstration of return-to-zero signaling in both OOK and DPSK formats to improve receiver sensitivity in an optically preamplified receiver," *1999 IEEE LEOS Annu. Meet. Conf. Proceedings. LEOS'99. 12th Annu. Meet. IEEE Lasers Electro-Optics Soc. 1999 Annu. Meet. (Cat. No.99CH37009)*, vol. 1, pp. 226–227, 1999.
[19] J. C. Juarez, D. W. Young, J. E. Sluz, and L. B. Stotts, "High-sensitivity DPSK receiver for high-bandwidth free-space optical communication links," *Opt. Express*, vol. 19, no. 11, p. 10789, 2011.
[20] M. Pfennigbauer, M. Pauer, P. J. Winzer, and M. M. Strasser, "Performance Optimization of Optically Preamplified Receivers for Return-to-zero and Non Return-to-zero Coding," *AEU - Int. J. Electron. Commun.*, vol. 56, no. 4, pp. 261–267, 2002.
[21] C. Fuchs, C. Schmidt, F. Moll, D. Giggenbach, and A. Shrestha, "system aspects of optical LEO-to-ground links," *Int. Conf. Sp. Opt. 2016*, no. October, p. 25, 2017.
[22] International Telecommunications Union, "Optical Fibres, Cables and Systems," pp. 144–147, 2009.
[23] G. Artaud, N. Védrenne, R. Le Bidan, M. Velluet, and L. Pailler, "Physical layer performance assessment of free-space optical communications links," pp. 253–259, 2017.